8th Biennial International Conference
& Exposition on Petroleum Geophysics

"HYDERABAD 2010"

P-238

Recent Advances in Shallow Water Marine CSEM Surveying

Anh Kiet Nguyen[1], Friedrich Roth[1] and Håkon Pedersen[2]*
[1]*EMGS ASA, Norway*
[2]*EMGS Asia Pacific, Malaysia*

Summary

A new robust data-driven method for enhancing the marine CSEM subsurface response is presented. The method is demonstrated to enhance resolution and depth of penetration significantly, particularly in shallow water of 100m depth or less.

Introduction

In the very early attempts to use marine controlled source electromagnetic (CSEM) measurements for hydrocarbon exploration, it was considered to be a deep water exploration technology (Eidesmo et al. 2002). This was mainly caused by the reduced *relative* response from thin resistive layers in shallow water. However, these conclusions were based on examples where the deep water response was tenfold. Since then, it has become obvious that much smaller responses can be significant. Recent theoretical investigations reveal that sufficient subsurface response for detection of thin resistive layers is usually present also in shallow water. Mittet (2008) showed that anomalous responses could be seen in very shallow waters (40 meters), and Weiss (2007) concluded that transient measurements in 100 meters of water can detect targets at 2 km burial depth.

From a more practical point of view, significant improvements of the acquisition technology as well as data processing, modelling and inversion algorithms must be made in order to fully exploit the capability of CSEM for imaging subsurface resistivity in shallow water environments.

Conventional CSEM source equipment has been designed for deep water operations. Hence an important development that must take place is on the source side. A typical conventional source configuration is similar to the one shown in Figure 1 *but without the buoys*. In this case, the electrodes are towed around 30m above the seabed and positioned acoustically. However, in shallow water (< 60m) precise positioning of the electrodes becomes difficult and the risk of impact with seabed or subsea installation becomes significant. Figure 1 shows a newly developed surface-towed source with GPS postioning more appropriate for shallow water CSEM surveys. This source configuration allows operation at water depth as low as 15m. Furthermore, it has a more stable source pitch and more accurate electrode positioning compared to conventional source configurations. Note that, for a 1D model with 100m of seawater over a 1 Ωm formation with a 50m thick 50 Ωm reservoir at 2000m depth, the scattered field from the reservoir actually *increases* for most source-receiver offsets for the surface-towed source configuration compared to the conventional seabed-towed source configuration.

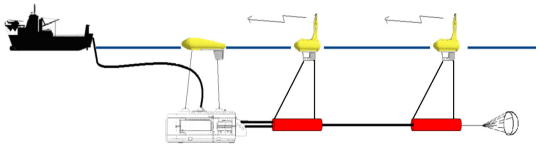

Figure 1: Schematic picture of a surface-towed electric dipole source appropriate for shallow water CSEM surveys. The grey box at the lower left is the towfish providing the source current to the electrodes. Buoys and electrodes are marked in yellow and red, respectively.

Shallow water also impacts finite-difference based modeling tools, since the modeling problem now becomes a multi-scale problem. To properly describe sources and receivers in a shallow water layer one must use dense modeling grids, which will cause memory and computational time problems if one also wishes to model deep buried resistive structures. Another problem is the airwave, which dominates the measured signal in shallow water. Thus the airwave must be modeled with high accuracy such that the modeling error is well below the weak response from deep buried resistive structures. Detailed descriptions of the improved modeling algorithm based on the fast finite-difference time-domain modelling algorithm (Maaø 2007) will be reported elsewhere.

On the data analysis and inversion side, several methods have been proposed to attenuate the dominance of the airwave in the measured data and thereby enhance the subsurface response in a shallow water environment. Among these are up-down separation (Amundsen et al. 2006), usage of azimuth data (Løseth and Amundsen 2007), and by applying spatial de-convolution methods (van den Berg et al. 2008). One often encountered challenge with methods aimed at enhancing the subsurface response is the requirement to measurement accuracy. In order to extract information which constitute a small fraction of the total signal, the subtraction process must be done with a very high degree of accuracy. It is therefore important to find enhancement methods for the subsurface response that involves as little uncertainty as possible. We now present a new technique for enhancing the CSEM subsurface response which shows a particularly large potential in shallow water environments and that involves a minimum degree of uncertainty.

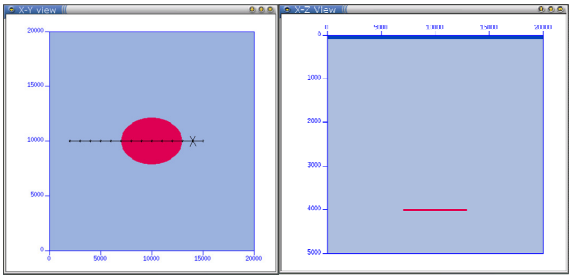

Figure 2: The model used in the numerical example study consists of 100 meters of water, a homogenous background formation, and a 50 m thick resistive body. The resistivities are 0.3, 2, and 50 Ωm respectively. The maximum length of the resistive body is 6 km, while the maximum width is 4 km. The burial depth of the resistive body is varied between 3 and 4 km. The left figure shows a horizontal cross-section at target depth and the black line indicates the synthetic survey layout with dots at receiver positions. The receiver position used for the numerical examples is marked with a cross. The right figure displays a vertical cross-section.

Theory

The significance of any measured physical quantity, F^{obs}, can be accessed by comparing its deviation from some hypothetical value, F^{synth}, with its uncertainty, ΔF^{obs}. This is often expressed in terms of an L2-norm misfit function

$$\varepsilon = \frac{\left|F^{obs} - F^{synth}\right|^2}{\left|\Delta F^{obs}\right|^2} \equiv \frac{\left|F^{obs} - F^{synth}\right|^2}{\alpha^2\left|F^{obs}\right|^2 + \left|n_F\right|^2} \qquad (1)$$

The uncertainty, ΔF^{obs}, typically consists of two parts; one multiplicative term, here represented with $\alpha\left|F^{obs}\right|$ and one additive term, $\left|n_F\right|$. The multiplicative uncertainty typically arises from uncertainties in the acquisition parameters (source amplitudes, positions, orientations etc.) where the *uncertainty in the measured values is proportional to the measured values themselves*. The additive uncertainty is due to noise or other uncertainties that do not depend on the measured values. Such uncertainty can be caused by the instrumentation or any external uncontrolled signals/noise. For marine electromagnetic measurements external noise sources can be due to natural radiation, swell and sea water currents. A typical requirement for having a significant deviation between the quantities F^{obs} and F^{synth} is $\varepsilon > 1$. A significant deviation between two scenarios then depends both on the sensitivity of F towards changes in the subsurface and on the measurement precision.

Often sensitivity can be enhanced by using derived quantities. However, derived quantities often involve an increase in uncertainty and this may reduce the overall benefit. Consider the electric field measured at two different frequencies but on the *same* channel and with the *same* source position and orientation. If we now consider a linear combination of these, the multiplicative uncertainty of the linear combination will be proportional to the linear

combination itself and not the original field. Thus, if we define

$$F(\omega) = E(\omega + \Delta\omega) - E(\omega) \qquad (2)$$

the multiplicative uncertainty will be proportional to $F(\omega)$ and *not* $E(\omega)$. The electric field values, $E(\omega)$, are assumed to be normalized with source strength and phase. The quantity defined in equation (2) can show a high degree of subsurface sensitivity. For later reference these types of quantities will be referred to as *frequency differenced field* which can be also be interpreted in terms of the transient impulse response since

$$F(\omega) \approx \Delta\omega\, \partial_{\omega} E(\omega) = \Delta\omega \int_0^{\infty} dt\ (it)\ E(t)\ e^{i\omega t} \qquad (3)$$

Thus, it emphasizes late-coming "events" in the signal and can show a high degree of subsurface sensitivity. Furthermore, in shallow water, the frequency differenced field strongly attenuates early events as for example the primary airwave. Assuming 1D layered models and water depths < 100m, it can be shown that the frequency differenced field attenuates more than 95% of the primary airwave while leaving responses from deep resistivity contrasts more or less unaltered. In the following we will show some basic results from 3D modelling and a synthetic case study with inversion. Based on this we will discuss the potential for this method.

Modeling example

Synthetic data was created using 3D modeling (Maaø 2007). The first set of models consist of 100 meters of 0.3 Ωm water, a homogenous 2 Ωm background formation, and a 50m thin 50 Ωm resistive body with elliptic shape. The resistive body has semi axes of 6 and 4 km in the x- and y-direction respectively and its burial depth is varied. Figure 2 shows the model with the resistive body at 4 km burial depth.

To examine the sensitivity towards the presence of the resistive body, we normalize (divide) with data from a model without the resistive body present. Figure 3 shows the normalized amplitudes and phases as a function of offset for the inline electric field and the frequency differenced field at some selected frequencies. Only very small changes in magnitudes and phases can be seen for the normal inline electric field. Typically, the magnitude change is less than a few percent, while the phase change is less than a few degrees. The frequency differenced field, however, shows a much larger sensitivity to the presence of the target. For Figure 3 the frequency difference used is 0.1 Hz. The sensitivity generally decreases when the frequency separation increases.

As shown in Figure 3, the frequency differenced field shows a great increase in sensitivity with respect to target sensitivity. However, the relevance of this sensitivity should be accessed through the misfit function, as defined in equation (1). For simplicity, the multiplicative uncertainty is set to 5% ($\alpha = 0.05$) of the inline electric field, and only the noise level, $|n_F|$, is varied. The square root of the misfit function is shown for various situations in Figure 4. We refer to this quantity as the *weighted sensitivity*. The effective noise levels used in these examples are $|n_F| = 1.0\times10^{-14}$ and 1.0×10^{-15} V/Am^2. While the normal inline data shows little response to the target and is not much affected by the effective noise level, the frequency differenced field shows a much higher weighted sensitivity. This is particularly true for the smallest effective noise levels. At the very low noise levels the weighted sensitivities can be larger by more than one order of magnitude.

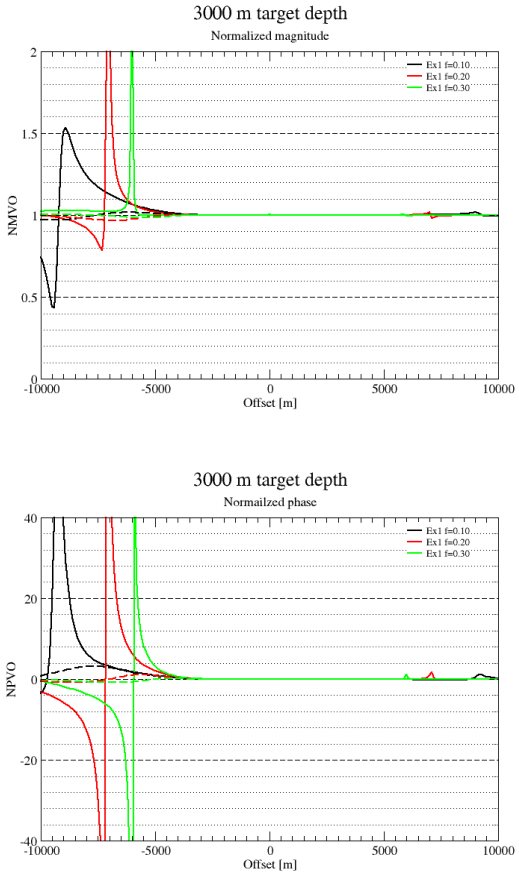

Figure 3: The plots show normalized responses for a target depth of 3000 meters at 100 meters of water depth. Normalized magnitudes are shown on top while normalized phases are shownat the bottom (degrees). The responses of the frequency differenced field are shown in solid lines while the inline electric field responses are shown in dashed lines. The frequency separation used to produce the frequency differenced field is 0.1 Hz.

Inversion example

The misfit function defined in equation (1) was implemented in 2.5D inversion (Hansen and Mittet 2009) using both the conventional inline electric field *E* and the frequency differenced field defined in equation (2). Two inversion schemes were implemented; one with only the inline electric field in the misfit and one where the frequency differenced field, equation (2) was added into the misfit, in addition to the inline electric field. We test the performance of the misfit functions using synthetic data from the 3D model shown in Figure 5.

The model consists of a highly resistive basement (150 Ωm) with large lateral variation in burial depth and large uplifts (two bodies) into the nearby overburden. The model also includes two layers of relatively high resistivity of 6 and 10 Ωm just below the target. The target (100 Ωm) is a 100m thick and nearly elliptical shape at a 45 degree angle to the towline. It is approximately 2km wide, 4km long under the towline. The target depth is 3km and the resistivity of the overburden is 2 Ωm. The water depth is 100m. The towline cross section of the model is shown in Figure 5. The numerical grids were 50x50x100m^3 in the 3D modeling and 50x100 m^2 in the 2.5D inversion. In the inversion, the four layers below the target and the water layer are inverted as areas of homogeneous resistivity while the rest of the model is inverted pixel by pixel. We use the background model, same model without the reservoir, as the starting model. Weak smoothness regularization is applied to stabilize the inversion. The frequencies selected where 0.1, 0.2 and 0.3 Hz with equal amplitudes,

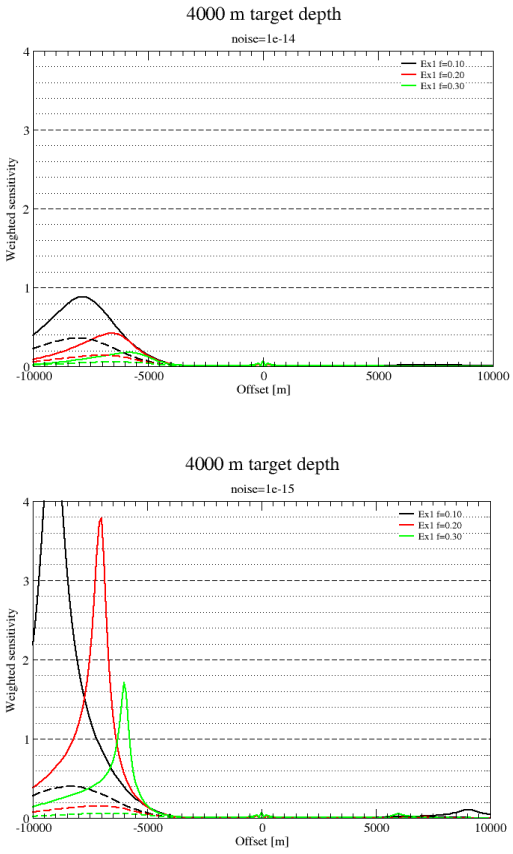

Figure 4: The figure shows numerical results for weighted sensitivity as a function of source-receiver offset for different noise levels and a target depth of 4000 meters. The dashed lines refer to weighted sensitivities for the inline electric field, while the solid lines refer to weighted sensitivities for the frequency differenced data. The difference in frequencies was set to 0.1 Hz.

$\alpha = 0.05$ and $|n_F| = 3.0\times10^{-15}$ V/Am^2. White noise with amplitude 3.0×10^{-15} V/Am^2 is added to the data prior the inversion.

Figure 6 shows the inverted models using the frequency differenced misfit and the conventional misfit. We see in Figure 6 that 2.5D inversion with the frequency differenced misfit puts in a resistivity anomaly at the correct depth. The anomaly was shifted slightly laterally due to the 3D shape of the reservoir that is not accounted for in a 2.5D inversion scheme. Thus, the horizontal position of the inverted resistive target is more in agreement with the center of the 3D target than with the position of the target at the given cross section. In contrast to this, 2.5D inversion using the conventional misfit is not able to find any resistivity anomaly. We also notice that the frequency differenced misfit function provides much better resistivity of the constrained layers when comparing with the true model. In both cases, the average misfit for the inverted models corresponds to an average data error of 3%.

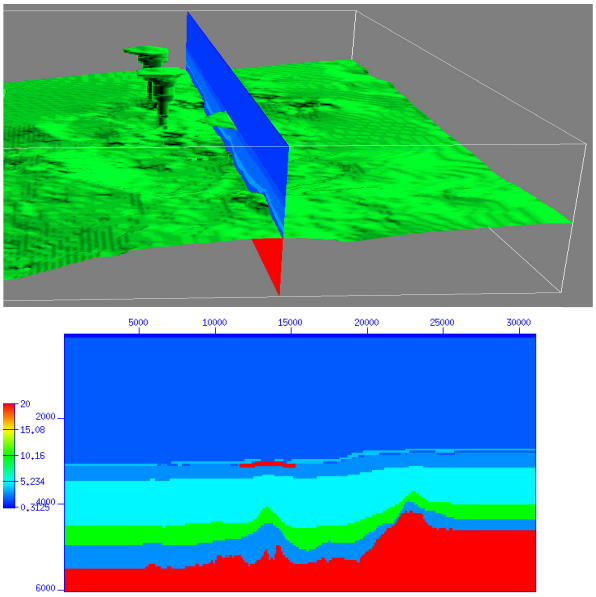

Figure 5: Top: 3D model showing the high resitive (150 Ohm m) basement with uplifts, the reservoir and the towline. Bottom: 2D slice along the towline of the 3D resistivity model.

In order to minimize uncertainty, the proposed method assumes data acquired on the same receiver channel with signals emitted at the same source position and orientation. The latter can be obtained by emitting at two or more frequencies simultaneously. The only multiplicative uncertainty left, which is proportional to the original frequency dependent data, is therefore due the

measurement of the source current and the calibration of the signal at the given frequencies. Note that any known systematic error in the frequency components can be compensated for and will not generate additional uncertainty. As shown in Mittet (2008), the scattered field caused by the presence thin resistive layers are usually larger in shallow waters than in deeper waters. Thus, aiming at methods to completely remove the sea surface interaction also means to reduce the magnitude of the scattered field. For sufficiently small or deep structures the scattered field may therefore end up below the effective noise floor. In the presented examples, the scattered field in the frequency differences has been of similar magnitude as for the scattered field of the single frequencies.

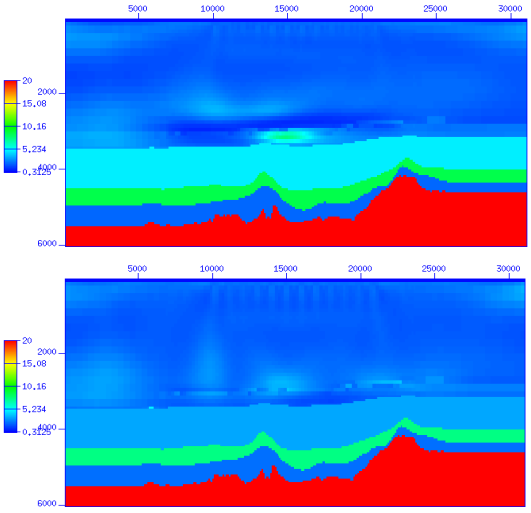

Figure 6: Top: Inverted model after adding frequency differenced cost function to the conventional cost function. Bottom: Inverted model using conventional cost function.

Conclusions

By utilizing frequency differencing we have found that a significant improvement in depth of penetration and resolution can be achieved. This is particularly true in a shallow water environment. The method requires a sufficiently high signal to noise ratio.

References

Amundsen, L., L. Løseth, R. Mittet, S. Ellingsrud, and B. Ursin, 2006, Decomposition of electromagnetic fields into upgoing and downgoing components; Geophysics, **71**, no. 5, G211–G223.

Eidesmo, T., S. Ellingsrud, L. M. MacGregor, S. Constable, M. C. Sinha, S. Johansen, F. N. Kong, and H. Westerdahl, 2002, Sea bed logging (SBL) a new method for remote and direct identification of hydro carbon filled layers in deepwater areas; First Break, **20**, 144–152.

Hansen, K. R., and Mittet, R., 2009, Incorporating seismic horizons in inversion of CSEM data; *SEG Expanded Abstracts*, **28**, 694-698

Løseth, L. O., and L. Amundsen, 2007, Removal of air-responses by weighting inline and broadside CSEM/SBL data; *SEG Expanded Abstracts*, **26**,529–533.

Maaø, F. A., 2007, Fast finite-difference time-domain modelling for marine subsurface electromagnetic problems; Geophysics, **72**, no. 2, A19–A23.

Mittet, R., 2008, Normalized amplitude ratios for frequency-domain CSEM in very shallow water; First Break, **26**, 47–54.

Van den Berg, P. M., A. Abubakar, and T. M. Habashy, 2008, Removal of sea-surface wavefields and source replacement in CSEM data processing; *SEG Expanded Abstracts*, **27**, 672–675.

Weiss, C., 2007, The fallacy of the "shallow-water problem" in marine CSEM exploration; Geophysics, **72**, no. 6, A93–A97.

Acknowledgements

We would like to thank EMGS for permission to publish the results and Frank Maaø at Statoil for his contribution to the development of the frequency differencing method.